Ferroelectric Barium Titanate Nanocubes as Capacitive Building Blocks for Energy Storage Applications

Saman Salemizadeh Parizi,[†] Axel Mellinger,[‡] and Gabriel Caruntu*,[†]

[†]Department of Chemistry and Biochemistry and the Science of Advanced Materials (SAM) Program, Central Michigan University, Mt. Pleasant, Michigan 48858, United States

[‡]Department of Physics and the Science of Advanced Materials (SAM) Program, Central Michigan University, Mt. Pleasant, Michigan 48858, United States

S Supporting Information

ABSTRACT: Highly uniform polymer−ceramic nanocomposite films with high energy density values were fabricated by exploiting the unique ability of monodomain, nonaggregated $BaTiO_3$ colloidal nanocrystals to function as capacitive building blocks when dispersed into a weakly interacting dielectric matrix. Monodisperse, surface-functionalized ferroelectric 15 nm $BaTiO_3$ nanoparticles have been selectively incorporated with a high packing density into poly(vinylidene fluoride-*co*-hexafluoropropene) (P(VDF-HFP)) leading to the formation of biphasic $BaTiO_3$−P(VDF-HFP) nanocomposite films. A systematic investigation of the electrical properties of the nanocomposites by electrostatic force microscopy and conventional dielectric measurements reveals that polymer−ceramic film capacitor

structures exhibit a ferroelectric relaxor-type behavior with an increased intrinsic energy density. The composite containing 7% $BaTiO_3$ nanocrystals displays a high permittivity (ε = 21) and a relatively high energy density (E = 4.66 J/cm^3) at 150 MV/m, which is 166% higher than that of the neat polymer and exceeds the values reported in the literature for polymer−ceramic nanocomposites containing a similar amount of nanoparticle fillers. The easy processing and electrical properties of the polymer−ceramic nanocomposites make them suitable for implementation in pulse power capacitors, high power systems and other energy storage applications.

KEYWORDS: *barium titanate, ferroelectrics, nanocrystals, capacitor, energy storage*
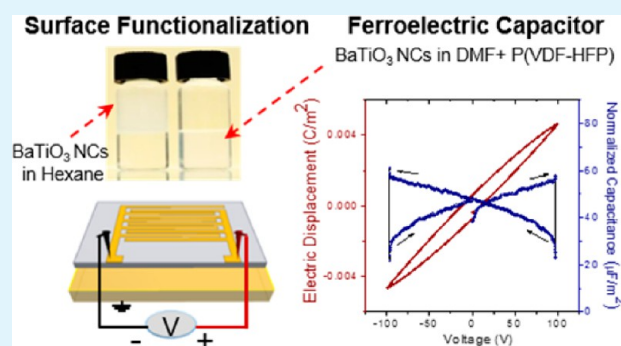
1. INTRODUCTION

With the continuous trend toward miniaturization in computing and electronics and the increasing popularity of electric and hybrid electric vehicles and portable electronic devices, there is a stringent need to develop advanced energy storage materials with increased energy and power densities, enhanced safety and structural stability, extended life cycles, and substantially reduced fabrication costs. Unlike conventional energy storage devices, such as fuel cells, electrochemical supercapacitors, and batteries, capacitors possess much higher power densities and ultrafast discharge speeds, typically in the order of milliseconds or microseconds,[1−4] which make them the leading candidates for niche applications in clean energy technologies. These include but are not restricted to the design of pulsed power and holdup devices, output filtering systems in communications, power supplies in gas and oil exploration, advanced decoupling capacitors, and transmitter power supplies in the aerospace industry and solar and/or wind modules.[5−7] Although the current state-of-the-art capacitors possess high power densities (10^7 W/kg), the released energy density values are relatively low, as they result from the fundamental limitations of the constituent linear dielectric materials.[8] The

energy density recoverable from a dielectric material in a capacitor geometry is described as

$$U_e = \int E dD \tag{1}$$

where E is the applied external electric field, and D stands for the electric displacement, that is, the total charge density induced by applying an external electric field (E).[9,10] In linear dielectric materials, the energy density is proportional to the relative dielectric constant ε_r and the square of the breakdown electric field E_b:

$$U_e = 0.5\varepsilon_r\varepsilon_0 E_b{}^2 \tag{2}$$

where ε_0 is the vacuum permittivity constant (ε_0 = 8.85 × 10^{-12} F/m).[11] According to eqs 1 and 2, a high energy density can be recovered from materials with a high dielectric constant which can withstand a high electric field. Polymer materials, such as polystyrene, polypropylene, polyimides, poly(phenyl quinoxa-

line), polyethylene terephthalate, poly(methyl methacrylate), epoxy resins, poly(arylene ether), and poly(arylene ether oxazole) have been used for the design of capacitors due to their unique combination between a high breakdown strength and high solution processability, durability, light weight, flexibility, and relatively low fabrication cost.[12] However, with few exceptions, they present a linear dielectric behavior associated with relatively low dielectric constant values and, therefore, low energy densities. For example the dielectric constant of biaxially oriented polypropylene (BOPP) films is only ε = 2.2, which drastically limits the energy density and energy storage capacity of these materials.[13,14] Unlike linear dielectrics, ferroelectric materials present much higher values of the dielectric permittivity, in particular in the vicinity of ferroelectric-paraelectric phase transition, as well as a dielectric nonlinearity.[11,14−17] Such high dielectric constant values are typically associated with high electrical displacements, thereby making ferroelectrics excellent candidates for the design of the next generation capacitors for energy storage applications.[8−12] From this viewpoint, one roadblock in implementing bulk ferroelectric ceramics such as barium titanate ($BaTiO_3$) or polyvinyldene fluoride (P(VDF))-based ferroelectric polymers and its copolymer poly(vinylidenefluoride-co-trifluoroethylene) (P(VDF-TrFE)) in highly efficient energy storage systems is the fact that the high remanent polarization results in up to 60% unreleased energy because of the large hysteresis resulted upon charging the capacitor.[3,10,18] Many efforts have been made in the recent years to design dielectric polymer−ceramic nanocomposites with high permittivity, low dielectric loss, and sufficiently high breakdown strength for energy storage applications. These high permittivity polymer−ceramic nanocomposites have been obtained by either embedding $BaTiO_3$ nanoparticles with variable sizes (typically ranging from 8 to 70 nm) into a polymer matrix,[13,19−21] also known as 0−3 nanocomposites, or coating them with a polymer shell in a core−shell geometry.[22−25] The volume fraction of the filler nanoparticles in the polymer−ceramic nanocomposite was varied between 0 and 50%. The dielectric constant was found to increase with the ceramic content and generally varied between 29.5 and 110, whereas the breakdown strength was found to follow an opposite trend.

Recently, it has been suggested that the discharged energy density of a polymer can be significantly improved by scaling down the size of the ferroelectric domains to the nanometer-length scale. In such a case, the cooperative coupling between the domains decreases significantly, thereby resulting in the hardening of the D-E loops and the increase of the efficiency of these energy storage materials. As an example, Yang et al. showed that the irradiation of P(VDF-TrFE) crystals with an electron beam induces a ferroelectric-relaxor behavior associated with nanoscale ferroelectric "pockets" created within the volume of the polymer surrounded by a weakly interacting dielectric matrix.[14] Owning to the synergistic effect caused by the increase of the distance between the P(VDF-TrFE) chains and their pinning, the constituent dipoles of these nanodomains can flip rapidly when subjected to an electric field. This will result into a decrease of the remanent polarization and an enhancement of the energy density of the polymer. In this work, we report on the rational design and characterization of a novel type of flexible hybrid organic−inorganic nanocomposites with superior dielectric performance by using monodomain aggregate-free ferroelectric $BaTiO_3$ colloidal nanocrystals[26] as capacitive building blocks. The resulting nanocomposites were

characterized by using electrostatic force microscopy (EFM) combined with conventional electric measurements in a capacitor geometry.

By uniformly dispersing the nanoscale fillers into a dielectric poly(vinylidene fluoride-co-hexafluoropropene) (P(VDF-HFP)) polymeric matrix, the resulting 0−3 $BaTiO_3$−P(VDF-HFP) nanocomposite films harness the electrical properties of the pristine phases; that is the high ε_r of the ceramic fillers along with the high DC-breakdown strength of the polymer matrix, respectively. In such structures the electrical dipoles of individual ferroelectric nanocrystals do not interact with each other but can flip rapidly when an electric field is applied. This unique feature, combined with the linear response of the dielectric matrix, allow these nanocomposites to mimic a ferroelectric relaxor-type behavior, that is, narrow P versus E hysteresis loops, which enhance remarkably the discharged energy density, making these systems very attractive for application in energy storage.

2. EXPERIMENTAL SECTION

2.1. Surface Functionalization of $BaTiO_3$ Cuboidal Nanocrystals. In a typical process, 5 mL of a hexane colloidal solution of $BaTiO_3$ nanocubes dispersion was combined with 5 mL of $NOBF_4$ (5 mM) in dimethylformamide (DMF) at room temperature. The resulting mixture was stirred until the nanocubes were transferred from the hexane solution into DMF across the interface between the polar and nonpolar phases. Powdered P(VDF-HFP) (Aldrich; translucent pellets containing less than 15% HFP) was dissolved in the DMF solution of $BaTiO_3$ nanocubes. The resulting clear solutions were cast and/or spin coated onto different substrates thereby yielding highly uniform $BaTiO_3$−P(VDF-HFP) nanocomposite films with various thicknesses. The resulting film samples were heat-treated at 120 °C for 2 h in air.

2.2. Characterization. The morphology and internal structure of $BaTiO_3$ nanocubes and polymer−ceramic nanocomposites were studied by transmission electron microscopy (TEM) with a JEOL-2010 microscope, scanning electron microscopy (SEM) with a JEOL JSM-7500F microscope and powder X-ray diffraction (XRD) with a Panalytical X'Pert 3040 MPD diffractometer from working with Cu Kα radiation. Fourier-transform infrared (FTIR) spectroscopy experiments were performed at room temperature with a Thermo Scientific Nicolet 380 spectrometer, whereas thermal analysis was performed with a TA-SDT Q600 instrument using a heating rate of 5 °C/min under flowing N_2.

2.3. Scanning Probe Microscopy. The polarization switching, local ferroelectric and dielectric response of materials were studied at room temperature with an Asylum Research MFP-3D atomic force microscope using a platinum/titanium coated cantilever (AC240TM, nominal spring constant ~2 N/m, resonance frequency ~70 kHz). The PFM measurements were performed on $BaTiO_3$ nanocrystals dispersed onto an indium tin oxide (ITO) glass substrate by applying a high-frequency modulating voltage to the tip. The EFM images were collected by lifting the tip at a distance of 20 nm from the surface of the 50 nm-thick polymer−ceramic film. The nanocomposite contains 5% volume fraction of 15 nm $BaTiO_3$ nanoparticles and was deposited by spin-coating at a speed of 3000 rpm for 30 s on an ITO/glass substrate.

2.4. Device Fabrication and Measurements. Ferroelectric capacitor devices have been fabricated in both parallel plates and interdigital electrode geometry by using 10 μm-thick $BaTiO_3$−P(VDF-HFP) nanocomposite films spin-cast on polyimide (Kapton) substrates followed by the deposition of 50 nm thick Au electrodes via a thermal evaporation process. Interdigital microelectrodes were subsequently fabricated by photolithography with a positive photo-resist (Shipley S1813) and ion-milling (ATC ORION-IM) for the etching process. The normalized capacitance, electric displacement, and energy density values of biphasic nanocomposites with different volume fractions (2−7%) of $BaTiO_3$ ferroelectric filler nanoparticles

were measured using a Premier II tester (Radiant Technologies, Inc.) in a capacitor geometry. Frequency-dependent dielectric constant value measurements of the nanocomposites films with the top and bottom electrodes were performed by using an Agilent 4284A Precision LCR Meter with a working frequency ranging from 20 Hz to 1 MHz at 1 Vrms.

3. RESULTS AND DISCUSSION

3.1. Synthesis of Ferroelectric Monodisperse Aggregate-Free BaTiO$_3$ Nanocubes.
Because one important limitation of the performance of polymer–ceramic nanocomposites in energy storage applications is related to the improper dispersion of the high surface energy filler nanoparticles into the continuous low surface energy dielectric polymer matrix, we take advantage of the high quality of cuboidal BaTiO$_3$ colloidal nanocrystals synthesized by our group using a phase-transfer method under solvothermal conditions.[31] Without the uniformity in the size and shape of the nanoparticles and their proper surface modification, large aggregates often form when nanoparticles are dispersed into a polymer matrix, leading to high values of the dielectric loss and leakage, which will substantially affect the dielectric characteristics of the nanocomposite material.[27−30] To alleviate this problem, many groups tried to develop highly reliable synthetic routes for the preparation of perovskite ceramic nanocrystals, but success in this area has been sparse. The as-prepared nanocrystals are nearly monodisperse, with sizes that can be varied from 5 to 70 nm and retain oleic acid (OA) molecules on their surfaces, which enable them to organize into hierarchical structures, such as self-assemblies, superlattices, and superparticles. We also recently demonstrated that the BaTiO$_3$ nanocubes retain a tetragonal distortion associated with a polar ordering to a size down to 5 nm, which makes them excellent candidates for the design of polymer–ceramic nanocomposites for various applications in electronics and energy storage.[26] Figure 1 displays the transmission electron
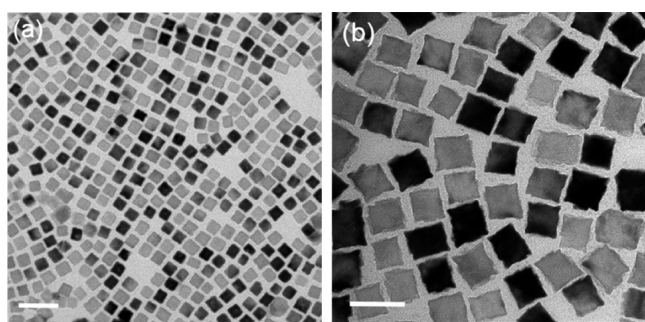

Figure 1. Top-view TEM images of (a) 15 nm and (b) 35 nm BaTiO$_3$ nanocubes obtained by a phase transfer method under solvothermal conditions (scale bars, 50 nm).

microscopy (TEM) micrographs of BaTiO$_3$ nanocubes with sizes of 15 and 35 nm, respectively. The BaTiO$_3$ nanocubes are surface passivated with oleic acid molecules, and they present uniform sizes and shapes, indicating that they can be used as building blocks for the design of high energy density polymer–ceramic nanocomposites. To characterize the ferroelectric properties of the BaTiO$_3$ nanocubes, we performed preliminary piezoresponse force microscopy (PFM) experiments in dual AC resonance tracking (DART) mode.[32,33]

Piezoresponse force microscopy is a powerful scanning probe technique for mapping the ferroelectric domains at the nanoscale and studying the local polarization switching in which variations in the orientation of the polarization can be distinguished through changes in the phase of the piezoelectric deformation of the sample subjected to the action of an oscillating electric field. As seen in the PFM phase contrast image (Figure 2d) obtained of an individual 35 nm BaTiO$_3$ nanocrystal and amplitude/phase versus bias voltage plots (Figure 2a,b,e,f) for both the 15 and 35 nm nanocubes, stable ferroelectric switching characteristics occur at room temperature with a sharp transition between two opposite orientations of the polarization, that is, a 180° shift of the phase of the piezoelectric response in the presence of an external electric field. These experimental results corroborate well the data from high-resolution electron diffraction, indicating that the differently sized BaTiO$_3$ nanocubes present a ferroelectric monodomain state, and if dispersed into a nonpolar matrix, they will present a ferroelectric relaxor-type behavior.[26] The values of the out-of-plane piezoelectric coefficient (d_{33}) for the 15 and 35 nm BaTiO$_3$ nanocubes estimated from the fitting of the linear portion of amplitude-voltage butterfly loops are 8 and 14 pm/V, respectively. These values are smaller than that reported for single crystalline (d_{33} = 90 pm/V)[34] and bulk BaTiO$_3$ (d_{33} = 75 pm/V)[35] but are higher than those obtained for BaTiO$_3$ dots formed through nanosphere lithography with an edge length of 220 nm and a height of 40 nm (d_{33} = 2 pm/V). These experimental findings indicate a superior preservation of the piezoelectric properties for our colloidal nanomaterials. The relatively low values of the longitudinal piezoelectric coefficient can be ascribed to the preference of the dielectric polarization to adopt an in-plane orientation in order to minimize the depolarization energy.[33,36]

3.2. Surface Functionalization of Aggregate-Free Monodisperse BaTiO$_3$ Nanocubes.
Monodisperse, single domain ferroelectric BaTiO$_3$ nanocubes were used as fillers for the design of highly uniform biphasic nanocomposites for energy storage applications. To this end 15 nm BaTiO$_3$ nanocubes have been used as ferroelectric fillers, whereas the copolymer poly(vinylidene fluoride-co-hexafluoropropene) (P-(VDF-HFP)) was used as a host matrix. One important problem associated with the design of high-quality polymer–ceramic nanocomposites for energy storage is related to dispersing the nanoparticles into the polymer host and therefore preventing the filler aggregation and formation of voids. As such, the surfaces of the nanocrystals should be adequately tailored to achieve a high compatibility between their polarity and that of the polymer. The chemical synthesis used in this work yields high-quality hydrophobic BaTiO$_3$ nanocrystals, which are generally immiscible with polar polymers such as P(VDF-HFP). Therefore, to enhance the compatibility between the nanofiller and the matrix and to produce solution-processable high-performance nanocomposite films for energy storage applications, the oleic acid molecules should be replaced by hydrophilic species, either ionic or molecular. Dong and co-workers recently proposed a generalized strategy for the sequential surface functionalization of various types of nanocrystals by replacing the oleic acid capping agent molecules with inorganic charged ligands, such as the BF$_4^-$ ions.[37] This simple ligand exchange reaction occurs very quickly when a hexane solution containing the BaTiO$_3$ nanoparticles is mixed with an *N,N*-dimethylformamide (DMF) solution of nitrosonium tetrafluoroborate for NOBF$_4$. It is worth mentioning that the ligand exchange process is accompanied by the formation of a slightly acidic medium as
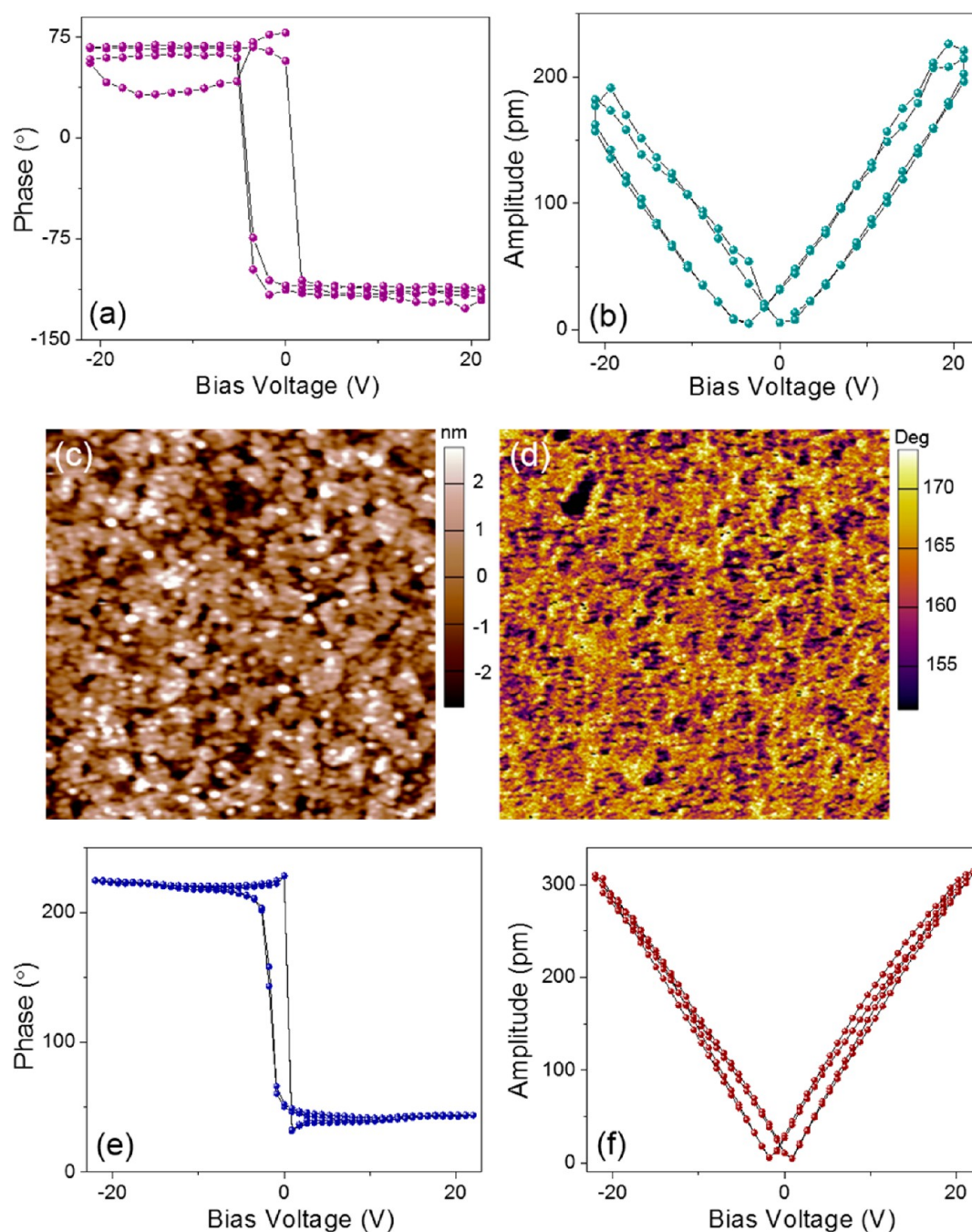
Figure 2. Piezoresponse force microscopy (PFM) phase and amplitude plots for (a and b) 15 nm and (e and f) 35 nm BaTiO$_3$ nanocrystals. (c) Topography AFM and (d) phase contrast PFM images of the 35 nm BaTiO$_3$ sample. The scan area was 3 × 3 μm.

a result of the reaction of NO$_2$ and water, which may lead to the dissolution of BaTiO$_3$ nanoparticles by the protons present in the solution if the amount of NOBF$_4$ in the DMF solution is not adjusted carefully. Figure 3a shows the schematic of an individual oleic acid-capped BaTiO$_3$ nanocube before and after the ligand exchange process.

The first vial in the picture shows the mixture of the hexane solution containing the oleic acid-capped BaTiO$_3$ nanocubes (top layer) and a DMF solution of NOBF$_4$ (bottom layer). Owing to their different polarities, when mixed together, the hexane and DMF solutions form a two-phase mixture with the BaTiO$_3$ nanoparticles-containing solution phase as the top layer of the mixture (Figure 3a). However, if the two solutions are

shaken for a short period of time, a rapid ligand exchange process takes place, and the oleic acid molecules on the surface of the BaTiO$_3$ nanocubes are replaced by BF$_4^-$ ions. In such conditions, the BF$_4^-$-passivated BaTiO$_3$ nanocubes become hydrophilic and are transferred across the liquid−liquid interface into the polar phase (right vial in Figure 3a) while remaining nonaggregated due to the electrostatic repulsions between the negatively charged ligands. As seen in the TEM micrographs presented in Figure 3b,c, the morphology of the BaTiO$_3$ nanocrystals are not affected by the ligand exchange process; they remain separated with a smaller interparticle distance due to the shorter lengths of the BF$_4^-$ ions compared
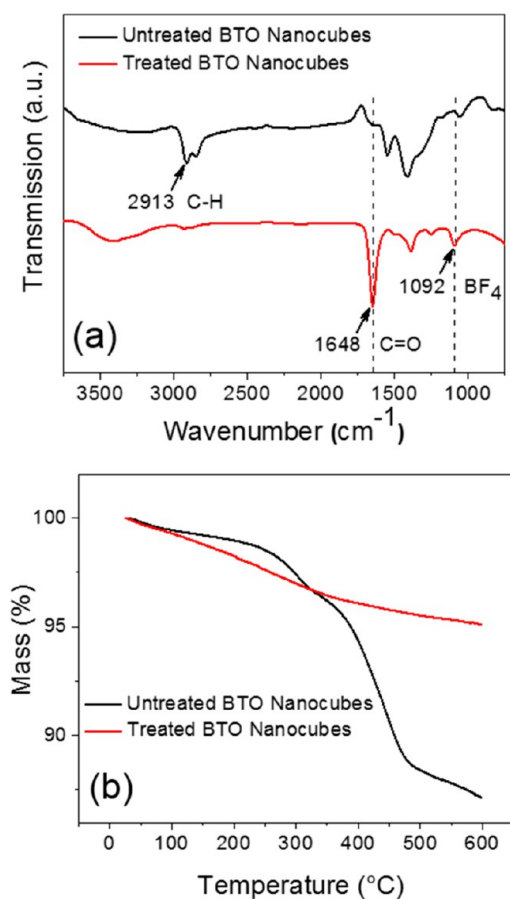
Figure 3. (a) Schematic illustration of the ligand-exchange process with $NOBF_4$ and photographs of the colloidal dispersions of 15 nm $BaTiO_3$ nanocubes in hexane and DMF. TEM images of the 15 nm $BaTiO_3$ nanocrystals (b) before and (c) after the $NOBF_4$ surface treatment (scale bars, 100 and 200 nm, respectively).

to the length of the hydrocarbonated chain of the carboxylic acid.

The resulting colloidal solutions of BF_4^--capped $BaTiO_3$ nanoparticles with sizes of 15 and 35 nm are stable in DMF solutions for several months without any noticeable aggregation of the nanoparticles, which further confirms the high quality of the nanocrystals obtained by this synthetic route. It is worth mentioning that DMF solutions of 15 nm $BaTiO_3$ nanocubes passivated with BF_4^- ions are more stable than those corresponding to 35 nm $BaTiO_3$ nanocrystals as a result of a greater surface-to-volume ratio and, consequently, the retention of an increased amount of capping agents on their surfaces. This directly affects the maximum solubility of the BF_4^--capped $BaTiO_3$ nanocrystals, which was found to decrease from 20 mg/mL for the 15 nm $BaTiO_3$ nanoparticles to 5 mg/mL for the 35 nm nanoparticles. The FTIR spectra of $BaTiO_3$ nanocubes before and after the ligand exchange process (Figure 4a) further confirm that the treatment of the colloidal dispersions of $BaTiO_3$ nanocrystals in hexane with a DMF solution of $NOBF_4$ successfully removed the oleic acid molecules. This is indicated by the substantial reduction of C−H stretching band at 2913 cm^{-1}, associated with the hydrocarbonated chain, in conjunction with the band at around 1092 cm^{-1} ascribed to the BF_4^- stretching mode,[37,38] while no bands attributed to NO$^+$ cations (∼2100−2200 cm^{-1}) have been observed in the FTIR spectrum. In excellent agreement

with the observations made by Dong et al., a new band located at 1648 cm^{-1}, corresponding to the C=O vibration in N,N-dimethylformamide, was observed in the FTIR spectrum of the $BaTiO_3$ nanopowders after the ligand exchange process, suggesting that both DMF molecules and BF_4^- ions passivated the surface of the $BaTiO_3$ nanocrystals as a result of the ligand exchange process. As seen in the TGA profiles of the as-synthesized and $NOBF_4$-surface modified $BaTiO_3$ nanocubes (Figure 4b), a mass reduction of a 3% was observed when the $BaTiO_3$ nanopowders obtained after the ligand exchange reaction with $NOBF_4$ were heated to 600 °C under a controlled atmosphere of N_2. Unlike the barium titanate nanopowders obtained after the $NOBF_4$ treatment, the TGA profile of the oleic-acid-capped $BaTiO_3$ nanocubes shows a significant mass loss around 350 °C, corresponding to a reduction in mass of the sample of about 13%. These experimental data corroborate well the results obtained by vibrational spectroscopy, which confirms that the bulky organic ligands can be easily replaced with BF_4^- anions and DMF molecules upon ligand exchange with a DMF solution of $NOBF_4$ at room temperature.

3.3. Fabrication and Characterization of $BaTiO_3$–P(VDF-HFP) Nanocomposite Films. The addition of a P(VDF-HFP) powder to the DMF solution of 15 nm surface modified single domain ferroelectric $BaTiO_3$ cuboidal nanocrystals under a vigorous stirring leads to the dissolution of the

Figure 4. (a) FTIR spectra of 15 nm BaTiO$_3$ nanocubes (black) before and (red) after NOBF$_4$ treatment; (b) TGA profiles of the BaTiO$_3$ nanopowder (black) before and (red) after the surface engineering process.
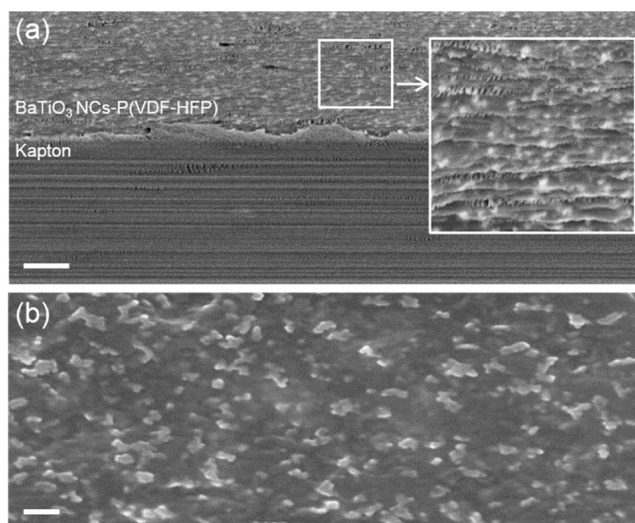

Figure 5. (a) Cross-sectional and (b) top view scanning electron microscopy (SEM) images of the BaTiO$_3$−P(VDF-HFP) nanocomposite film with 5% fillers spin coated on a Kapton substrate, (scale bars, 1 μm and 100 nm, respectively). (a, inset) Close-up images of the polymer−ceramic nanocomposite film.

polymer in the polar solvent. This also yields highly homogeneous biphasic nanocomposites without the need of sonication or high shear mixing as a result of the interaction between the fluorine ions in the copolymer host matrix and the oxide nanoparticles.[39] As shown in the top surface and cross-sectional SEM images of BaTiO$_3$−P(VDF-HFP) nanocomposites, smooth thin films containing 5% fillers were produced by spin-coating the DMF solutions of BaTiO$_3$−P(VDF-HFP) nanocomposites. The cross-sectional SEM image confirms that the nanoparticles are uniformly distributed within the polymer matrix, although some small aggregates were observed forming on the surface of the film sample, possibly due to the spin-coating process (Figure 5b). The volume fraction of the ferroelectric filler nanoparticles in the polymer matrix was kept relatively low, typically ranging from 2 to 7%. This is because it is well-known that large volume fraction of the oxide phase, as well as a large discrepancy in the dielectric permittivity of the filler and the matrix, substantially reduces the effective dielectric strength of the nanocomposite with an abrupt decrease of the breakdown strength around 10% and a gradual decrease for concentrations ranging between 20 and 50%[17] as a result of the enhancement of the average electric field in the host material.[40−45]

The local dielectric characterization of the BaTiO$_3$−P(VDF-HFP) nanocomposite films was performed by electrostatic force microscopy (EFM). Electrostatic force microscopy is a new and highly versatile scanning force microscopy-related

technique able to determine the spatial variation of the surface charge and the dielectric screening in various nanostructured materials with a nanometer resolution.[46−48] A typical EFM experiment is performed by a two-step procedure consisting of imaging the topography of the sample in AFM mode followed by the measurement of the electrostatic force gradient in the reverse scan. While the former measurements are carried out in tapping mode, the latter ones are performed by lifting the cantilever at a controlled distance, z, from the substrate plane (z = 10−100 nm), which leads to a capacitive coupling between the tip and the sample. During the EFM-scan, the tip oscillates in the vicinity of its resonance frequency (f_0), and the smallest variation on the capacitance between the tip and the substrate (C) will induce a frequency shift (Δf)[49,50] described by the relationship

$$\Delta f \approx \frac{f_0}{2k} \frac{\partial F}{\partial z} \tag{3}$$

where k and F are the spring constant of the cantilever and the capacitive tip−sample electrostatic force, respectively. The latter is defined by the equation

$$F = \frac{1}{2} \frac{\partial C}{\partial z} (V_{tip} - V_{surface})^2 \tag{4}$$

where C is the capacitance between the tip and the sample, and V_{tip} and $V_{surface}$ are the bias voltages applied to the tip and the surface, respectively. In a typical experiment, both positive (+8 and +4 V) and negative (−4 V) bias voltages were applied through the tip, whereas the film sample was biased at a constant voltage in such a way that the voltage applied to the surface remains constant ($V_{surface}$ = −8 V). Figure 6b,c shows the AFM height image and the EFM Δf data for a film capacitor obtained from a 50 nm thick BaTiO$_3$−P(VDF-HFP) nanocomposite film with a concentration of filler nanoparticles of 5% subjected to a bias voltage of +8 V. During the EFM measurement, the tip was lifted 20 nm above the surface of the film sample. The EFM image reveals the existence of a phase contrast between the BaTiO$_3$ filler nanoparticles and the
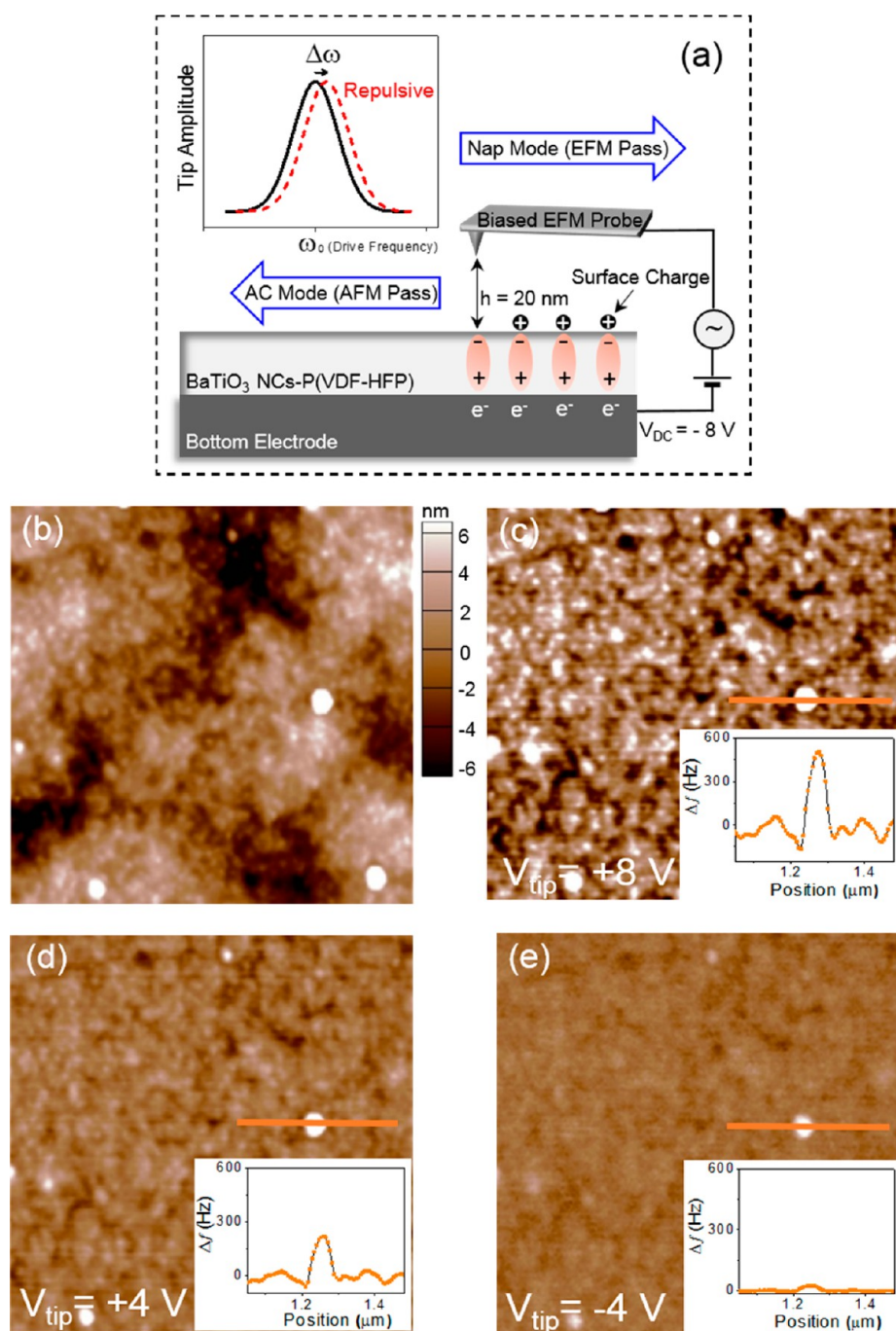
Figure 6. (a) Schematic illustration of the EFM technique and the frequency shift due to the surface polarization charge of the sample; (b) AFM topography image of the 15 nm BaTiO$_3$−P(VDF-HFP) film (5% filler concentration). The scan area was 1.2 × 1 μm. (c) Associated EFM data and frequency shift plot for V_{tip} = +8 V; EFM data and frequency shift plots for (d) V_{tip} = +4 V and (e) V_{tip} = −4 V.

P(VDF-HFP) host matrix with many dotted areas associated with the capacitive footprint of the BaTiO$_3$ nanoparticles which, unlike the polymer matrix, are responsive to the external electric field.

The phase contrast EFM images further confirm the high compositional uniformity of the biphasic nanocomposite film resulting from the uniform distribution of the nanocrystals into the polymer host matrix. The qualitative interpretation of the EFM data suggests that the white contrast areas corresponds to a positive phase shift, associated with positive charges on the surface of the nanocomposite film. These are likely due to the repulsive forces existing between the tip and the sample

originating from the particular orientation of the individual dipoles in the BaTiO$_3$ nanocrystals dispersed in the polymer matrix. For a small aggregate formed by the BaTiO$_3$ NCs on the surface of the nanocomposite, the magnitude of the frequency shift was found to be close to 500 Hz (Figure 6c) and decreased upon changing the bias voltage applied through the tip to +4 V and −4 V (Figure 6d,e) as a result of the lower value of the electric field applied to the sample. Interestingly, the capacitive electrostatic force between the film sample and the tip suggests that individual nanocubes possess a much higher capacitance or dielectric permittivity compared to those of the P(VDF-HFP) matrix. On the basis of these experimental
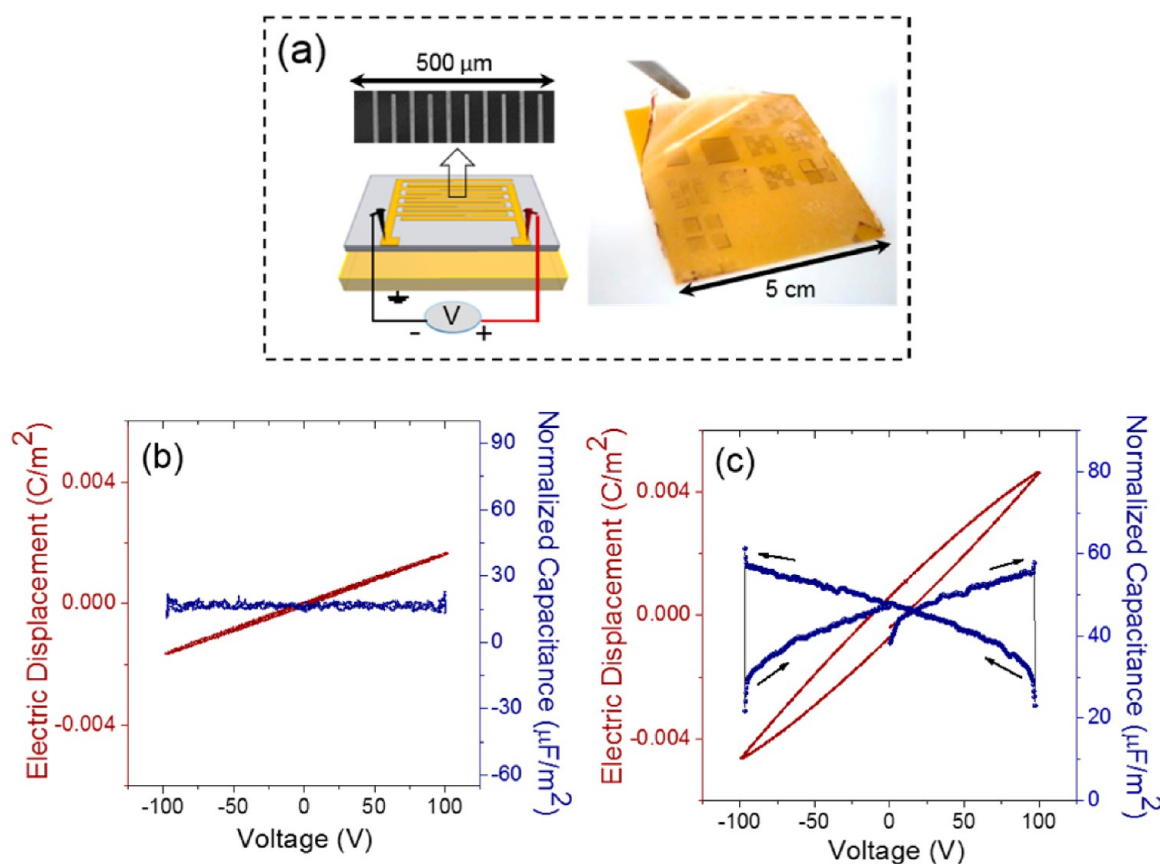
Figure 7. (a) Schematic and photograph of the capacitor geometry; (b, red) $D-V$ and (blue) $C-V$ characteristics for neat P(VDF-HFP) capacitor; (c, red) $D-V$ and (blue) $C-V$ characteristics for BaTiO$_3$–P(VDF-HFP) capacitor.

observations, we can undoubtedly conclude that the relatively homogeneous distribution of the polarization charge in the film is associated with the existence of isolated, well-dispersed individual BaTiO$_3$ nanocubes, which behave as capacitive building blocks in the P(VDF-HFP) host matrix.

The electrical properties of the polymer–ceramic nanocomposites have been studied in a capacitor geometry obtained upon deposition of 50 nm thick Au electrodes on BaTiO$_3$–P(VDF-HFP) films. For the qualitative assessment of the properties of the polymer–ceramic nanocomposite films measurements were performed using interdigitized microelectrodes, as this geometry leads to the highest possible signal-to-noise ratio. However, to quantitatively determine the energy density characteristics of the BaTiO$_3$–P(VDF-HFP) nanocomposites, we performed measurements in a parallel plate capacitor geometry. However, as shown in Figure S1 (Supporting Information), in the case of BaTiO$_3$–P(VDF-HFP) nanocomposite films with 5% filler nanoparticles, the dielectric displacement measurements in both parallel plate and interdigitated microelectrode geometry are similar. The optical image of a typical capacitor constructed on Kapton substrate shows a large area uniformity and good flexibility, which make these nanocomposites suitable for implementation into flexible electronics (Figure 7a). The electric displacement and normalized capacitance of the polymer–ceramic nanocomposite film-based capacitors were measured as a function of the bias voltage (100 V) and were compared with that of pristine P(VDF-HFP) capacitors. The linear D versus V dependence observed for a neat P(VDF-HFP)-based capacitor (Figure 7b) suggests that the polymer crystallizes in the nonpolar α phase,

the most usual polymorph, which is conventionally obtained when copolymer solutions are cast onto a desired substrate.[11,51] These findings were also confirmed by examining the powder XRD pattern, which features peaks ascribed to the α phase of the polymer host matrix (Figure S2 Supporting Information). As seen in Figure 7b, the normalized capacitance does not depend on the electric field and remains constant during the charging and discharging cycles, which is consistent with a linear dielectric behavior of the capacitor. Conversely, when 15 nm BaTiO$_3$ NCs are present in the P(VDF-HFP) matrix (5% volume fraction of ceramic filler), the charging (V increasing) curve does not trace the discharging (V decreasing) curve and, in tandem with the nonlinearity of the D versus V loop, indicates the existence of a hysteresis behavior of the polymer–ceramic nanocomposite (Figure 7c). Another salient characteristic of the biphasic nanocomposite is the narrowness of the hysteresis loop, with a remnant polarization close to zero. Moreover, the symmetrical butterfly shaped curve of the capacitance (Figure 7c) confirms the nonlinear dielectric response associated with the polarization rotation within the monodomain BaTiO$_3$ nanoparticles embedded into the polymer matrix.

Such nonlinear characteristics of the nanocomposite originate from the polar state of BaTiO$_3$ nanocrystals which are uniformly distributed into the host polymer matrix, thereby forming well-separated ferroelectric nanodomains. The narrowness of the D versus V loops strongly suggests that the electric properties of the nanocomposite are similar to those observed in ferroelectric relaxors such as irradiated P(VDF-TrFE) polymers[14] and poly(vinylidenefluoride-co-trifluoroethylene-

17513

dx.doi.org/10.1021/am502547h | *ACS Appl. Mater. Interfaces* 2014, 6, 17506–17517

chlorofluoroethylene) (P(VDF-TrFE-CFE))[3] which are conventionally associated with enhanced energy storage densities. On the basis of these preliminary data, we propose another type of efficient energy storage system consisting of noninteracting single domain ferroelectric nanoparticles uniformly distributed into dielectric matrix. To further confirm the ferroelectric relaxor state and perform a comprehensive study on the influence of the nanoparticle size on the macroscopic electrical properties of the polymer−ceramic nanocomposites, we are currently conducting high-frequency and temperature-dependent measurements of the dielectric polarization, and these results will be reported in a forthcoming paper.

The dielectric properties of the $BaTiO_3$−P(VDF-HFP) nanocomposite films were studied at room temperature using three series of samples containing different volume fractions of the ferroelectric filler nanoparticles, which typically varied from 2 to 7%. As we mentioned before, the concentration of the nanoparticles was kept below 10% to avoid both an abrupt drop in the breakdown strength of the nanocomposites and the aggregation of nanocubes within the composite, which can potentially lead to the increase of the hysteresis loss of the capacitor. Figure 8a illustrates the experimental results obtained
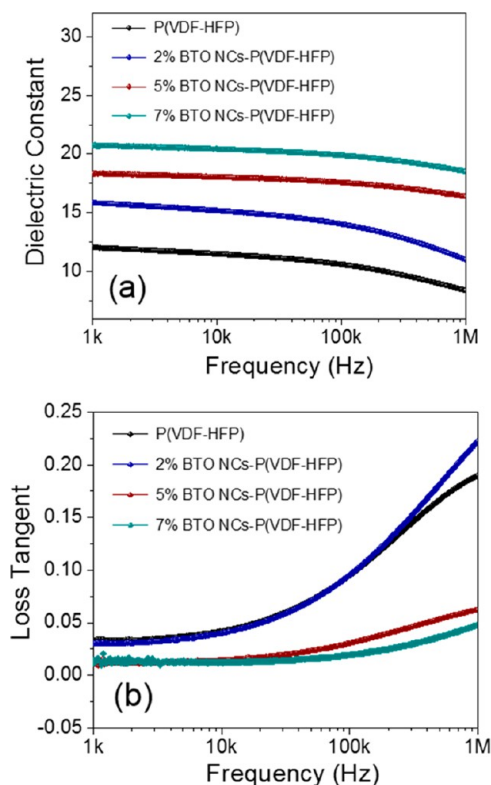

Figure 8. Frequency dependence of the dielectric properties of the polymer−ceramic nanocomposites with various volume fractions of the filler nanoparticles: (a) dielectric constant and (b) dielectric loss tangent.

by dielectric spectroscopy of the $BaTiO_3$−P(VDF-HFP) nanocomposite films with different volume fraction of 15 nm $BaTiO_3$ nanoparticles with the broadband frequency ranging from 1 kHz to 1 MHz. The dielectric constant of the nanocomposite was found to increase with increasing the concentration of the ferroelectric filler nanoparticles as a result of the higher dielectric permittivity of the ceramic nanoparticles. At the same time, the dielectric constant of the

biphasic nanocomposites decreases with the frequency due to the lower mobility of electrical dipoles in the high frequency regime. The dielectric permittivity reaches a maximum value of $\varepsilon = 21$ for polymer−ceramic films containing 7% $BaTiO_3$ nanoparticles at a fixed frequency of 1 kHz, which is a substantial increase compared to the measured value of the pristine copolymer P(VDF-HFP) phase ($\varepsilon = 11$). Figure 8b shows the frequency variation of the dielectric loss tangent (tan δ) of the $BaTiO_3$−P(VDF-HFP) nanocomposite films. The loss tangent decreases with increasing the amount of $BaTiO_3$ nanoparticles in the nanocomposite with a value close to 0.015 at 1 kHz for the nanocomposite film containing 7% $BaTiO_3$ nanoparticles. Although the dielectric loss can be generally affected by different factors, such as the direct current conduction, space charge migration, and dipole relaxation,[23,52] in the case of $BaTiO_3$−P(VDF-HFP) nanocomposite films, the reduction of the dielectric loss tangent has been ascribed to the restricted mobility of the molecular chains as a result of the presence of uniformly dispersed $BaTiO_3$ nanoparticles in the polymer host matrix. Specifically, the uniform dispersion of ferroelectric nanocrystals with a high surface-area-to-volume ratio into the P(VDF-HFP) matrix leads to the enhancement of the interfacial area of the nanocomposite. In turn, this will significantly limit the movement of the molecular dipoles, thereby inducing a decrease of the dipole relaxation of $BaTiO_3$−P(VDF-HFP) nanocomposite films.

To estimate the released energy density of $BaTiO_3$−P(VDF-HFP) nanocomposite films with various filler volume ratios, we measured the electric displacement as a function of the electric field by using capacitors with a parallel plate configuration (Figure S3 Supporting Information). The values of the released energy density of the pristine copolymer and the nanocomposites (Figure 9) were calculated by integrating the
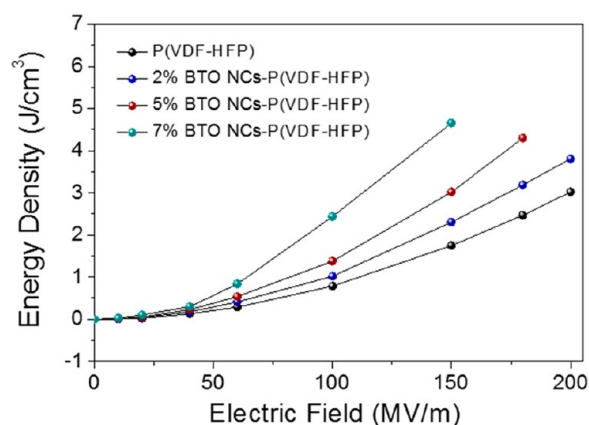

Figure 9. Variation of the released energy density of the biphasic nanocomposite with different volume fractions as a function of the electric field.

discharging D versus E loops. As such, the energy density of the biphasic nanocomposite with 7% volume ratio of $BaTiO_3$ nanoparticles is 4.66 J/cm³, which represents a 166% enhancement with respect to the energy density of the copolymer, whose value at 150 MV/m is close to 1.75 J/cm³. Last, but not least, the energy density value for the composite with 7% $BaTiO_3$ is in line with and exceeds the values reported in the literature for polymer−ceramic nanocomposites containing a similar amount of nanoparticle fillers. For example, Li et al. reported an energy density of 3.3 J/cm³ for $BaTiO_3$−

P(VDF-HFP) nanocomposites,[19] whereas Rahimabady et al. found a value close to 1 J/cm³ for core−shell BaTiO₃@TiO₂−P(VDF-HFP) nanocomposites[25] to enumerate just a few. However, in most cases, the size of the nanoparticles used was above 30 nm, which often induces aggregation and can be detrimental to the electrical proprieties of the composites.

The relatively low breakdown field values observed in our nanocomposites have been presumably assigned to a corona effect forming around individual dielectric nanocrystals dispersed into the polymer matrix mainly due to the conductive nature of the ionic species used as capping agents. Work is currently underway to fabricate/test BTO-polymer nanocomposites using oleic-acid-capped nanocrystals to increase the degree of dispersion of the nanocrystals into the polymer matrix and enhance the breakdown field values; the results will be reported in a forthcoming paper.

4. CONCLUSIONS

In summary, we propose a new concept for the rational design of polymer−ceramic nanocomposites with increased energy storage densities by using surface-modified monodomain ferroelectric BaTiO₃ nanoparticles uniformly dispersed into a solution-processable lightweight dielectric matrix of PVDF-HFP. The as-prepared monodisperse BaTiO₃ nanocubes are hydrophobic due to the retention of oleic acid molecules on their surfaces but can easily be rendered hydrophilic upon replacing the carboxylic acid with inorganic ions such as BF_4^- via a simple ligand exchange process in DMF. The resulting colloidal solutions are then mixed with a polar polymer, such as poly(vinylidene fluoride-*co*-hexafluoropropene) (P(VDF-HFP)), whereby the nanocrystals are uniformly dispersed into the polymer host matrix. The biphasic composite solution was cast onto various substrates, yielding very uniform and flexible polymer−ceramic nanocomposite films.

We show for the first time that the nanocrystal fillers separated from each other into the weakly interacting dielectric polymer matrix form ferroelectric nanodomains thereby leading to a macroscopic ferroelectric-relaxor behavior of the biphasic nanocomposite. Flexible and reproducible ferroelectric capacitors were fabricated from BaTiO₃−P(VDF-HFP) nanocomposites, and we demonstrated that they present a low hysteresis loss due to the high reversibility of the dielectric polarization of the BaTiO₃ nanocubes. The study of the individual BaTiO₃ nanocubes using electrostatic force microscopy at ambient temperature revealed that they behave as the capacitive building blocks with a high and uniform charge polarization on the surface of the capacitor. An increase of 166% of the energy density of the polymer was found when 15 nm BaTiO₃ nanocubes were uniformly dispersed into the host matrix; such a value is superior to those reported for similar systems with other polymers and much higher concentrations of the filler nanoparticles. The methodology of designing polymer−ceramic nanocomposites by using monodisperse single domain ferroelectric nanocrystals as capacitive building blocks is currently being extended to other nanoscale perovskite systems and polymer host matrices and will be reported in a forthcoming paper. This not only enables us to further optimize the capacitor energy densities, but also will allow these nanocomposites to be incorporated into energy storage functional devices.

■ ASSOCIATED CONTENT

ⓢ Supporting Information

X-ray diffraction patterns for BaTiO₃ nanocubes and nanocomposite, displacement versus the electric field for BaTiO₃−P(VDF-HFP) nanocomposites. This material is available free of charge via the Internet at http://pubs.acs.org.

■ AUTHOR INFORMATION

Corresponding Author
*E-mail: g.caruntu@cmich.edu.

Notes
The authors declare no competing financial interest.

■ REFERENCES

(1) Wu, Z. S.; Parvez, K.; Feng, X.; Müllen, K. Graphene-Based in-Plane Micro-Supercapacitors with High Power and Energy Densities. *Nat. Commun.* **2013**, *4*, 2487.

(2) Pech, D.; Brunet, M.; Durou, H.; Huang, P.; Mochalin, V.; Gogotsi, Y.; Taberna, P.-L.; Simon, P. Ultrahigh-Power Micrometre-Sized Supercapacitors Based on Onion-Like Carbon. *Nat. Nanotechnol.* **2010**, *5*, 651−654.

(3) Chu, B.; Zhou, X.; Ren, K.; Neese, B.; Lin, M.; Wang, Q.; Bauer, F.; Zhang, Q. M. A Dielectric Polymer with High Electric Energy Density and Fast Discharge Speed. *Science* **2006**, *313*, 334−336.

(4) Kui, Y.; Shuting, C.; Rahimabady, M.; Mirshekarloo, M. S.; Shuhui, Y.; Tay, F. E. H.; Sritharan, T.; Li, L. Nonlinear Dielectric Thin Films for High-Power Electric Storage with Energy Density Comparable with Electrochemical Supercapacitors. *IEEE Trans. Ultrason., Ferroelectr., Freq. Control* **2011**, *58*, 1968−1974.

(5) Landrock, C. K.; Kaminska, B. *High Temperature Polymer Capacitors for Aerospace Applications*, In Proceedings of the Design, Automation, & Test in Europe Conference & Exhibition, Dresden, Germany, March 8−12, 2010.

(6) Zhong, L.; Ailing, W.; Xin, L. *Method of Electromagnetic Frequency Spectrum and Its Application*, In Proceedings of the 2011 International Conference on Computer Distributed Control and Intelligent Environmental Monitoring (CDCIEM), February 19−20, 2011.

(7) Muyeen, S. M.; Shishido, S.; Ali, M. H.; Takahashi, R.; Murata, T.; Tamura, J. Application of Energy Capacitor System to Wind Power Generation. *Wind Energy* **2008**, *11*, 335−350.

(8) Ortega, N.; Kumar, A.; Scott, J. F.; Douglas, B. C.; Tomazawa, M.; Shalini, K.; Diestra, D. G. B.; Katiyar, R. S. Relaxor-Ferroelectric Superlattices: High Energy Density Capacitors. *J. Phys.: Condens. Matter* **2012**, *24*, 445901.

(9) Wang, Q.; Zhu, L. Polymer Nanocomposites for Electrical Energy Storage. *J. Polym. Sci., Part B: Polym. Phys.* **2011**, *49*, 1421−1429.

(10) Tang, H.; Sodano, H. A. Ultra High Energy Density Nanocomposite Capacitors with Fast Discharge Using Ba₀.₂Sr₀.₈TiO₃ Nanowires. *Nano Lett.* **2013**, *13*, 1373−1379.

(11) Zhu, L.; Wang, Q. Novel Ferroelectric Polymers for High Energy Density and Low Loss Dielectrics. *Macromolecules* **2012**, *45*, 2937−2954.

(12) Nalwa, H. S. *Handbook of Low and High Dielectric Constant Materials and Their Applications: Phenomena, Properties, and Applications*, 1st ed; Academic Press: San Diego, 1999.

(13) Nash, J. L. Biaxially Oriented Polypropylene Film in Power Capacitors. *Polym. Eng. Sci.* **1988**, *28*, 862−870.

(14) Yang, L.; Li, X.; Allahyarov, E.; Taylor, P. L.; Zhang, Q. M.; Zhu, L. Novel Polymer Ferroelectric Behavior via Crystal Isomorphism and the Nanoconfinement Effect. *Polymer* **2013**, *54*, 1709−1728.

(15) Seongtae, K.; Hackenberger, W.; Alberta, E.; Furman, E.; Lanagan, M. Nonlinear Dielectric Ceramics and Their Applications to Capacitors and Tunable Dielectrics. *IEEE Elect. Insul. Mag.* **2011**, *27*, 43−55.

(16) Tomer, V.; Manias, E.; Randall, C. A. High Field Properties and Energy Storage in Nanocomposite Dielectrics of Poly(vinylidene fluoride-hexafluoropropylene). *J. Appl. Phys.* **2011**, *110*, 044107.

(17) Kim, P.; Doss, N. M.; Tillotson, J. P.; Hotchkiss, P. J.; Pan, M.-J.; Marder, S. R.; Li, J.; Calame, J. P.; Perry, J. W. High Energy Density Nanocomposites Based on Surface-Modified BaTiO$_3$ and a Ferroelectric Polymer. *ACS Nano* **2009**, *3*, 2581−2592.

(18) Asadi, K.; de Leeuw, D. M.; de Boer, B.; Blom, P. W. M. Organic Non-Volatile Memories from Ferroelectric Phase-Separated Blends. *Nat. Mater.* **2008**, *7*, 547−550.

(19) Li, J.; Claude, J.; Norena-Franco, L. E.; Seok, S. I.; Wang, Q. Electrical Energy Storage in Ferroelectric Polymer Nanocomposites Containing Surface-Functionalized BaTiO$_3$ Nanoparticles. *Chem. Mater.* **2008**, *20*, 6304−6306.

(20) Almadhoun, M. N.; Bhansali, U. S.; Alshareef, H. N. Nanocomposites of Ferroelectric Polymers with Surface-Hydroxylated BaTiO$_3$ Nanoparticles for Energy Storage Applications. *J. Mater. Chem.* **2012**, *22*, 11196−11200.

(21) Liu, S.; Zhang, H.; Sviridov, L.; Huang, L.; Liu, X.; Samson, J.; Akins, D.; Li, J.; O'Brien, S. Comprehensive Dielectric Performance of Bismuth Acceptor Doped BaTiO$_3$ Based Nanocrystal Thin Film Capacitors. *J. Mater. Chem.* **2012**, *22*, 21862−21870.

(22) Lin, M.-F.; Thakur, V. K.; Tan, E. J.; Lee, P. S. Surface Functionalization of BaTiO$_3$ Nanoparticles and Improved Electrical Properties of BaTiO$_3$/Polyvinylidene Fluoride Composite. *RSC Adv.* **2011**, *1*, 576−578.

(23) Xie, L.; Huang, X.; Huang, Y.; Yang, K.; Jiang, P. Core@Double-Shell Structured BaTiO$_3$−Polymer Nanocomposites with High Dielectric Constant and Low Dielectric Loss for Energy Storage Application. *J. Phys. Chem. C* **2013**, *117*, 22525−22537.

(24) Yang, K.; Huang, X.; Zhu, M.; Xie, L.; Tanaka, T.; Jiang, P. Combining RAFT Polymerization and Thiol−Ene Click Reaction for Core−Shell Structured Polymer@BaTiO$_3$ Nanodielectrics with High Dielectric Constant, Low Dielectric Loss, and High Energy Storage Capability. *ACS Appl. Mater. Interfaces* **2014**, *6*, 1812−1822.

(25) Rahimabady, M.; Mirshekarloo, M. S.; Yao, K.; Lu, L. Dielectric Behaviors and High Energy Storage Density of Nanocomposites with Core-shell BaTiO$_3$@TiO$_2$ in Poly(vinylidene fluoride-hexafluoropropylene). *Phys. Chem. Chem. Phys.* **2013**, *15*, 16242−16248.

(26) Polking, M. J.; Han, M.-G.; Yourdkhani, A.; Petkov, V.; Kisielowski, C. F.; Volkov, V. V.; Zhu, Y.; Caruntu, G.; Paul Alivisatos, A.; Ramesh, R. Ferroelectric Order in Individual Nanometre-Scale Crystals. *Nat. Mater.* **2012**, *11*, 700−709.

(27) Siddabattuni, S.; Schuman, T. P.; Dogan, F. Dielectric Properties of Polymer−Particle Nanocomposites Influenced by Electronic Nature of Filler Surfaces. *ACS Appl. Mater. Interfaces* **2013**, *5*, 1917−1927.

(28) Cheng, L.; Zheng, L.; Li, G.; Zeng, J.; Yin, Q. Influence of Particle Surface Properties on the Dielectric Behavior of Silica/Epoxy Nanocomposites. *Phys. B* **2008**, *403*, 2584−2589.

(29) Polizos, G.; Tomer, V.; Manias, E.; Randall, C. A. Epoxy-based Nanocomposites for Electrical Energy Storage. II: Nanocomposites with Nanofillers of Reactive Montmorillonite Covalently Bonded with Barium Titanate. *J. Appl. Phys.* **2010**, *108*, 074117.

(30) Schuman, T. P.; Siddabattuni, S.; Cox, O.; Dogan, F. Improved Dielectric Breakdown Strength of Covalently Bonded Interface Polymer−Particle Nanocomposites. *Compos. Interfaces* **2010**, *17*, 719−731.

(31) Adireddy, S.; Lin, C.; Cao, B.; Zhou, W.; Caruntu, G. Solution-Based Growth of Monodisperse Cube-Like BaTiO$_3$ Colloidal Nanocrystals. *Chem. Mater.* **2010**, *22*, 1946−1948.

(32) Brian, J. R.; Clint, C.; Sergei, V. K.; Roger, P. Dual-Frequency Resonance-Tracking Atomic Force Microscopy. *Nanotechnology* **2007**, *18*, 475504.

(33) Xie, S.; Gannepalli, A.; Chen, Q. N.; Liu, Y.; Zhou, Y.; Proksch, R.; Li, J. High Resolution Quantitative Piezoresponse Force Microscopy of BiFeO$_3$ Nanofibers with Dramatically Enhanced Sensitivity. *Nanoscale* **2012**, *4*, 408−413.

(34) Zgonik, M.; Bernasconi, P.; Duelli, M.; Schlesser, R.; Günter, P.; Garrett, M. H.; Rytz, D.; Zhu, Y.; Wu, X. Dielectric, Elastic, Piezoelectric, Electro-Optic, and Elasto-Optic Tensors of BaTiO$_3$ Crystals. *Phys. Rev. B: Condens. Matter Mater. Phys.* **1994**, *50*, 5941−5949.

(35) Jona, F.; Shirane, G. *Ferroelectric Crystals*, 1st ed.; Dover Publications: New York, 1993.

(36) Schilling, A.; Bowman, R. M.; Catalan, G.; Scott, J. F.; Gregg, J. M. Morphological Control of Polar Orientation in Single-Crystal Ferroelectric Nanowires. *Nano Lett.* **2007**, *7*, 3787−3791.

(37) Dong, A.; Ye, X.; Chen, J.; Kang, Y.; Gordon, T.; Kikkawa, J. M.; Murray, C. B. A Generalized Ligand-Exchange Strategy Enabling Sequential Surface Functionalization of Colloidal Nanocrystals. *J. Am. Chem. Soc.* **2010**, *133*, 998−1006.

(38) Lutz, H. D.; Himmrich, J.; Schmidt, M. Lattice Vibration Spectra. Part LXXXVI. Infrared and Raman Spectra of Baryte-type TlClO$_4$, TlBF$_4$, and NH$_4$BF$_4$ Single Crystals and of ^{11}B-Enriched NH$_4$BF$_4$. *J. Alloys Compd.* **1996**, *241*, 1−9.

(39) Nguyen, V. S.; Badie, L.; Lamouroux, E.; Vincent, B.; Santos, F. D. D.; Aufray, M.; Fort, Y.; Rouxel, D. Nanocomposite Piezoelectric Films of P(VDF-TrFE)/LiNbO$_3$. *J. Appl. Polym. Sci.* **2013**, *129*, 391−396.

(40) Huang, C.; Zhang, Q. Enhanced Dielectric and Electromechanical Responses in High Dielectric Constant All-Polymer Percolative Composites. *Adv. Funct. Mater.* **2004**, *14*, 501−506.

(41) Gilbert, L. J.; Schuman, T. P.; Dogan, F. Dielectric Powder/Polymer Composites for High Energy Density Capacitors, In *Advances in Electronic and Electrochemical Ceramics*, Vol. 179; Dogan, F., Kumta, P., Eds. John Wiley & Sons, Inc., Hoboken, NJ, 2012.

(42) Dasgupta, S. Polypropylene Filled with Barium Titanate: Dielectric and Mechanical Properties. *J. Appl. Polym. Sci.* **1978**, *22*, 2383−2386.

(43) Bai, Y.; Cheng, Z.-Y.; Bharti, V.; Xu, H. S.; Zhang, Q. M. High-Dielectric-Constant Ceramic-Powder Polymer Composites. *Appl. Phys. Lett.* **2000**, *76*, 3804−3806.

(44) Ma, D.; Siegel, R. W.; Hong, J.-I.; Schadler, L. S.; Mårtensson, E.; Önneby, C. Influence of Nanoparticle Surfaces on the Electrical Breakdown Strength of Nanoparticle-Filled Low-Density Polyethylene. *J. Mater. Res.* **2004**, *19*, 857−863.

(45) Lee, K. H.; Kao, J.; Parizi, S. S.; Caruntu, G.; Xu, T. Dielectric Properties of Barium Titanate Supramolecular Nanocomposites. *Nanoscale* **2014**, *6*, 3526−3531.

(46) McMorrow, J. J.; Cress, C. D.; Affouda, C. A. Charge Injection in High-κ Gate Dielectrics of Single-Walled Carbon Nanotube Thin-Film Transistors. *ACS Nano* **2012**, *6*, 5040−5050.

(47) Cuniot-Ponsard, M. Kelvin Probe Force Microscopy and Electrostatic Force Microscopy Responses to the Polarization in a Ferroelectric Thin Film: Theoretical and Experimental Investigations. *J. Appl. Phys.* **2013**, *114*, 014302.

(48) Coffey, D. C.; Ginger, D. S. Time-Resolved Electrostatic Force Microscopy of Polymer Solar Cells. *Nat. Mater.* **2006**, *5*, 735−740.

(49) Riedel, C.; Arinero, R.; Tordjeman, P.; Lévêque, G.; Schwartz, G. A.; Alegria, A.; Colmenero, J. Nanodielectric Mapping of a Model Polystyrene-Poly(vinyl acetate) Blend by Electrostatic Force Microscopy. *Phys. Rev. E: Stat., Nonlinear, Soft Matter Phys.* **2010**, *81*, 010801.

(50) Nguyen, H. K.; Prevosto, D.; Labardi, M.; Capaccioli, S.; Lucchesi, M.; Rolla, P. Effect of Confinement on Structural Relaxation in Ultrathin Polymer Films Investigated by Local Dielectric Spectroscopy. *Macromolecules* **2011**, *44*, 6588−6593.

(51) Lee, S. Crystal Structure and Thermal Properties of Poly-(vinylidene fluoridehexafluoropropylene) Films Prepared by Various Processing Conditions. *Fibers Polym.* **2011**, *12*, 1030−1036.

(52) Yang, K.; Huang, X.; Huang, Y.; Xie, L.; Jiang, P. Fluoro-Polymer@BaTiO$_3$ Hybrid Nanoparticles Prepared via RAFT Polymerization: Toward Ferroelectric Polymer Nanocomposites with High Dielectric Constant and Low Dielectric Loss for Energy Storage Application. *Chem. Mater.* **2013**, *25*, 2327−2338.

17517

dx.doi.org/10.1021/am502547h | *ACS Appl. Mater. Interfaces* 2014, 6, 17506−17517